Electromagnetic shower profile measurements in iron with 500 MeV electrons

N. Akchurin[a],[1], A.S. Ayan[a],*, N. Conan[b], I. Dumanoğlu[c], A. Fontaine[b],
J-P. Merlo[a], A. Muller[b], L. Rinolfi[b]

[a] *Department of Physics and Astronomy, University of Iowa, Iowa City, IA 52242, USA*
[b] *CERN, Geneva, Switzerland*
[c] *Cukurova University, Department of Physics, Adana, Turkey*
,

Abstract

The longitudinal and lateral shower profiles for 500 MeV electrons in iron are studied using dosimetry and activation techniques. The results are compared with Monte Carlo simulations and other previously published data. The agreement between the data and the *EGS4* simulation results is good; a simple shower profile parametrization of type $kz^{\alpha-1}\exp(-\beta z)$ does not represent the experimental data well at and around the shower maximum. The differences observed in the activation and dose profiles clearly show the role of photons in electromagnetic showers. The photon fraction increases as the shower develops deeper and they carry a larger energy fraction farther into the absorber. Photodisintegration reactions are responsible for the activation of the iron and we identified Mn^{54}, Fe^{53} and Mn^{56} as more active isotopes among several others. These studies were performed for estimating the dose and its profile for the CMS quartz fiber calorimeter radiation damage work performed at LIL (CERN). © 2001 Elsevier Science B.V. All rights reserved.

1. Introduction

There is a pressing need for radiation damage and activation analyses studies for the detectors planned at the Large Hadron Collider (LHC), particularly because some of them will experience

several hundreds of megarads during their useful lifetime. The forward calorimeters especially will face unprecedented particle fluxes. In the Compact Muon Solenoid (CMS) experiment, for example, at $\eta = 5$ in ~ 10 years of LHC operation, the forward calorimeters are expected to experience ~ 1 Grad of dose [1].

The CMS forward calorimeter consists of multi-mode synthetic silica-core optical fibers embedded in an iron absorber. The details of this type of a calorimeter can be found in Refs. [1,2]. In order to study the response of the forward calorimeter

---

*Corresponding author. Tel.: +1-319-335-2832; fax: +1-319-335-1753.

E-mail address: ahmet-ayan@uiowa.edu (A.S. Ayan).

[1] Now at Department of Physics, Texas Tech University, Lubbock, TX 79409, USA.

under these intense radiation conditions, we first performed dose and activation measurements in iron absorbers after having them irradiated with a 500 MeV electron beam at the LEP pre-injector (LPI) facility at CERN. We made Monte Carlo calculations to compare them with the data in an attempt to generalize and to use these results for the radiation damage studies of the prototypes irradiated at the same facility.

The details of the lateral and longitudinal dose profiles in the calorimeter absorber determine the magnitude and the extent of the radiation damage in quartz fibers. The radiation dose degrades the optical transmission in quartz fibers and worsens the response of the detector. In the 400–500 nm range, for example, the irradiation induced transmission loss reaches ~ 1 dB/m for 100 Mrads for most synthetic silica-core and fluorine-doped silica-clad fibers.

The CMS forward calorimeter absorber material(s) will get activated under intense LHC radiation fields. After 2 months of running at an average luminosity (5×10^{33} cm^{-2} s^{-1}) and a day of cool-down period, the activation level is estimated to be several thousand μS/h at the higher rapidity region. In addition to safety and maintanence concerns, this background introduces noise into the calorimeter system. In the case of the iron absorber (Fe I), as this study shows, ~ 110 Mrad of dose due to electrons results in 6.5 MBq of total activity at the shower maximum after about an hour of cool down.

In Section 2, we describe the two iron absorber structures that we constructed. The LPI beam properties are listed in Section 3. The dosimetry and activation analyses are discussed in Sections 4 and 5, respectively. The *EGS4* Monte Carlo results are presented together with the dosimetry and activation analyses. We summarize the results in the last section.

2. The iron absorber structures

2.1. First iron matrix (Fe I)

Fig. 1 shows the structure of the first iron matrix. The total length of the absorber is 206 mm (11.36X_0), deep enough to fully contain 500-MeV electron showers. The iron plates are positioned normal to the beam direction; the first four plates are 1 cm and the last eight are 2 cm thick with respect to the beam direction. They measure 40 mm $\times$ 40 mm on a side. Between each plate, a 0.5-mm thick (0.396 g/cm^2) Fe plate and a radiation sensitive (RISO)[2] [3] paper are placed. RISO paper consists of a thin plastic film containing a radiochromic dye (leucocyanide) which induces intense permanent colors when exposed to ionizing radiation. Like most cyanides, luecocyanide is colorless but upon irradiation, the cyanide bond is broken and the positive carbonium ion becomes colored. The 0.5-mm thick Fe plates were used for the activation measurements and the RISO sheets registered the integrated dose. These thin Fe plates are of identical chemical composition as the thicker ones. There was no air gap between the plates and/or the RISO paper.

2.2. Second iron matrix (Fe II)

The second iron matrix was constructed in order to study the lateral shower development in a wider range in detail, thus the transverse absorber dimensions measured 16 cm $\times$ 16 cm. In addition to the RISO papers sandwiched between plates, we embedded glass RadioPhotoLuminescent (RPL) dosimeters in small holes in some of the iron plates (indicated as shaded plates in Fig. 2). RPL technique is based on generation of color centers under irradiation in specially prepared glasses. These color centers can be activated by ultraviolet light and the subsequent luminescence can be recorded to indicate the absorbed dose. The glass samples we used were typically 0.5 mm in diameter and 5 mm in length. In addition, in order to investigate the characteristics of lateral activation profile, 0.5 mm thick and 1.5 cm diameter disks were placed inside the absorber as shown in Fig. 2. By this construction, we were able to measure the details of the lateral activation as well as longitudinal profiles, whereas with the first iron block (Fe I) we could only measure the total activation as a function of depth (Table 1).

---

[2] RISO stands for radiochromatic film dosimeter developed primarily by RISO National Laboratory, Roskilde, Denmark.
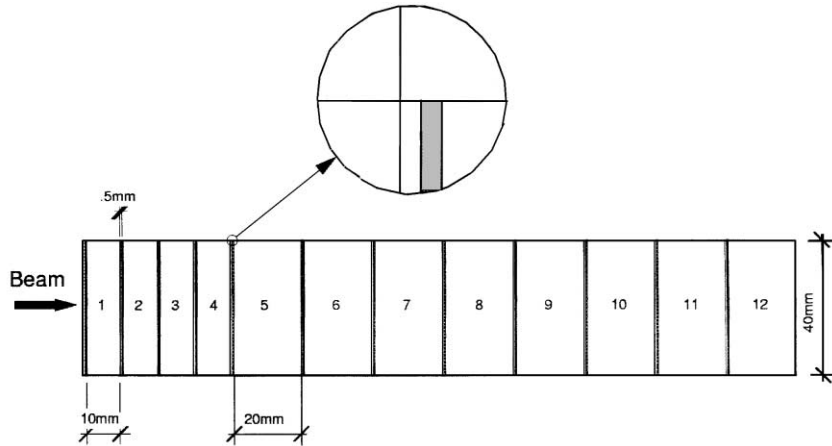
Fig. 1. The iron matrix consists of a sandwich of thin (0.5 mm) iron plates, sheets of radiation sensitive RISO paper (indicated as dark lines) and thicker iron plates (10 or 20 mm) as shown. Twelve such units make up the entire Fe I absorber matrix. The total depth of the stack is 206 mm, sufficient to contain all of the energy from 500 MeV electrons. The transverse dimensions are 40 mm × 40 mm.
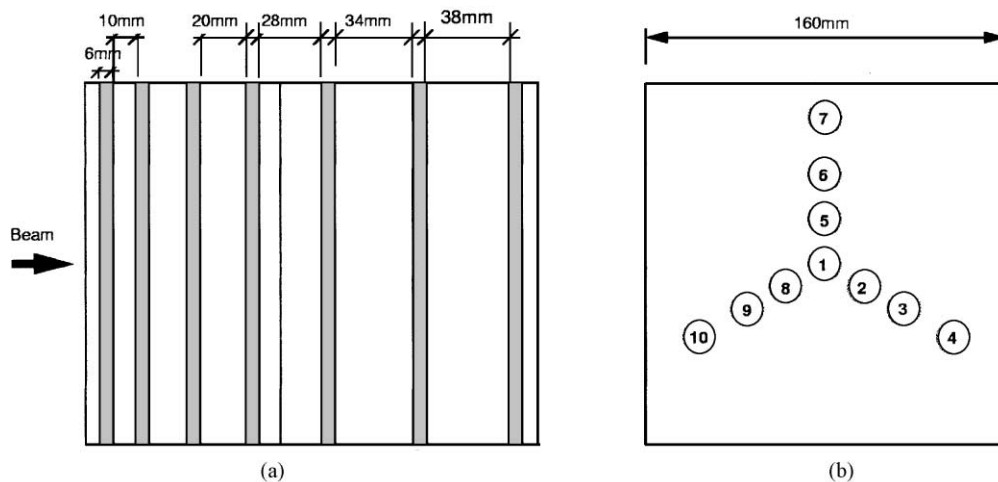

Fig. 2. (a) The second iron matrix (Fe II) consists of a sandwich of iron plates and sheets of radiation sensitive RISO paper. The RISO paper locations are shown in dark lines. The total depth of the stack is 200 mm. The transverse dimensions are 160 mm × 160 mm. (b) For lateral activation studies, we used a 0.5 mm thick sheets (shown as hatched lines in a), where 10 1.5 cm diameter disks were located in the shape shown. From the center (disk 1), the center of disks 2, 5, and 8 are at 2 cm, the disks 3, 6 and 9 are 4 cm and the disks 4, 7 and 10 are 6.5 cm away.

3. LPI beam

There is a 10-year time scale planned for the LHC experiments and the expected radiation doses are measured in many Mrads. The existing facilities that are able to provide comparable integarated doses in practicable times are low-energy but intense particle beams. One such facility is the LIL Experimental Area (LEA) at CERN [4], which can provide up to 700 MeV electrons in a dedicated facility of the LPI, downstream of the linac. The samples are

Table 1
The iron plates are composed of > 99% Fe and the impurities are estimated to total less than 1%. There is no Mn in the second absorber matrix

Block	C (%)	Mn (%)	P (%)	S (%)
Fe I	<0.10	<0.45	<0.035	<0.035
Fe II	<0.17	—	<0.045	<0.045

Table 2
Nominal beam parameters were used for this irradiation study. LPI can provide intense electron beams in a wide energy and intensity range and is especially well-suited for radiation damage studies of electromagnetic calorimeters. Note that beam sizes were slightly different for the first and the second iron block irradiations. We account for this difference in the simulation and dose calculations

Parameter	Range	Nominal (for these tests)
Energy (MeV)	180–700	500
Charge/pulse (e$^-$)	5×10^8–2×10^{10}	4×10^9
Frequency (Hz)	1–100	100
Pulse FWHM (ns)	10–40	10
RMS beam size (mm)	$\sigma_x = 3.3$–6.0	$\sigma_x(\text{FeI}) = 4.7$
		$\sigma_x(\text{FeII}) = 3.4$
	$\sigma_y = 3.3$–6.0	$\sigma_y(\text{FeI}) = 3.6$
		$\sigma_y(\text{FeII}) = 3.3$

placed on a remotely controlled table, 2 m downstream of a 0.1 mm (Al) thick vacuum window. Its contribution to the diffusion is 3.2 mm (RMS) in both planes at the location of the irradiation sample. The beam can be steered with a set of dipole magnets in a 10 cm × 10 cm area at the sample location. The integrated charge is measured by a beam position monitor just upstream of the exit vacuum window. Table 2 gives the nominal beam characteristics.

The first absorber matrix was exposed to beam for 3 h and 11 min, collecting 1.68×10^{15} electrons at a constant rate. The second iron block accumulated 2.73×10^{15} electrons in 34 min due to a higher number of cycles. The beam was centered at the geometric center of the absorber at all times.
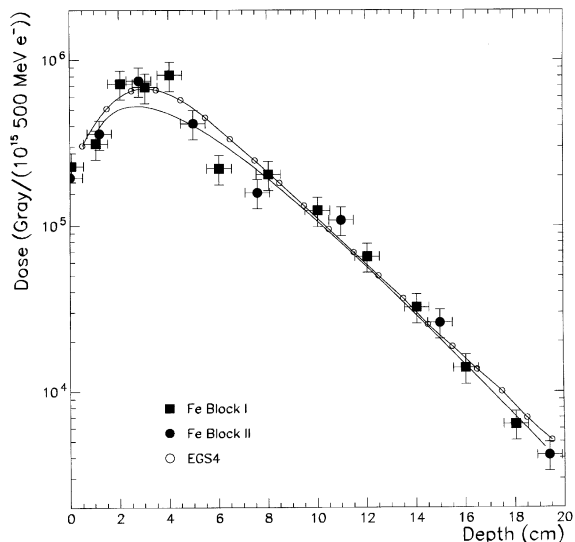

Fig. 3. The longitudinal shower dose profile for 500 MeV electrons in iron is measured using radiation sensitive (RISO) paper and represented by filled squares (Fe I) and circles (Fe II). The solid line is a fit to the data points which gives $\alpha = 2.14$ and $\beta = 0.42$ cm^{-1}. The connected open circles represent the *EGS4* simulation result. All values are normalized to 1.0×10^{15} electrons.

4. Dosimetry

RISO sheets were placed in the absorber structures (Figs. 1 and 2) and were analysed in 3 mm × 3 mm square grids. The typical precision of dose measurements using this technique is ±20%. The glass RPL dosimeters were placed in small holes in the absorber, as mentioned in Section 2, and later analyzed. We assume ±20% uncertainty in these measurements. The RPL dosimeters are well-suited and reliable at lower doses. We depended on RISO paper measurements for doses that exceed ∼ 1 KGy.

Fig. 3 shows the longitudinal development of 500 MeV electrons in iron. The dose is normalized to 1.0×10^{15} electrons and at the shower maximum, the total dose is ∼ 660 KGy. The data from Fe I and Fe II blocks are presented in the same figure. The longitudinal shower profile is usually expressed by a simple parametrization,

$$\frac{dE}{dz} = kz^{\alpha-1} \exp(-\beta z) \qquad (1)$$

where z refers to the longitudinal coordinate and k is a nomalization constant. The parameters α and β define the shower shape. The shower maximum takes place at $z_{\max} = (\alpha - 1)/\beta$.

The smooth solid line in Fig. 3 is a fit to the data points according to Eq. (1). As known, in the first few radiation lengths, this simplified expression neither represents the data nor the simulation results well [5]. When the first two data points are excluded from the fit, it suggests a shower maximum at 2.7 cm. The simulation however suggests $z_{\max} = 3.5$ cm as represented by the connected open circles in Fig. 3. The agreement between the data, fit and the simulation improves after $z \geqslant 4$ cm. The simplified fit to the shower shape, Eq. (1), should be viewed with some caution since it underestimates both the dose at the shower maximum by $\sim 40\%$ and its location, $z_{\max}$, by 20%.

Fig. 4 shows the development of shower at two different off-shower axis locations; 0.95 and 1.95 cm. The agreement between data and simulation results is good except the last two data points at 19 cm.
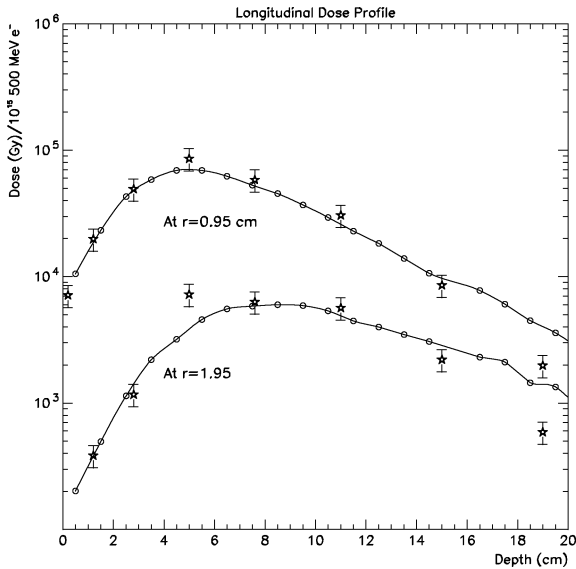
The characteristic parameter for lateral shower profiles is the Molière radius, R_{M}, and it is defined as

$$R_{\mathrm{M}} = \frac{E_{\mathrm{s}}}{E_{\mathrm{c}}} X_0, \qquad (2)$$

where $E_{\mathrm{s}} \approx 21.2$ MeV, E_{c} is the critical energy and X_0 is the radiation length. We take $E_{\mathrm{c}}^{\mathrm{Fe}} = 22.4$ MeV and $X_0^{\mathrm{Fe}} = 1.76$ cm.

On average, in one Molière radius ($R_{\mathrm{M}}^{\mathrm{Fe}} = 1.67$ cm), 90% of the energy is expected to be absorbed in an infinitely long absorber. 99% of the energy is absorbed in $3.5R_{\mathrm{M}}$. The electromagnetic shower consists of a narrow and energetic core, and a wide halo surrounds it. As the shower develops, the core broadens. The lateral shower development as a function of depth is shown in Fig. 5 for four different depths, 1 cm $(0.57X_0)$, 3 cm $(1.70X_0)$, 5 cm $(2.84X_0)$ and 15 cm $(8.52X_0)$. EGS4 [6] reproduces the RISO data well in all depths and RPL data up to 5 cm depth. However we have no explanation for the discrepancy between RPL data and the Monte Carlo at $z = 15$ and we will investigate this further in future. It is worthwhile to note that the energy threshold for gammas and electrons was set at 100 KeV and 1.5 MeV in EGS4, respectively, for this lateral development study. When these thresholds were reduced to 10 KeV for photons and 50 KeV for electrons, there was no appreciable difference. The lateral shower profile within one R_{M} is not significantly sensitive to these cuts; but it is natural to expect that these cuts would be important for $r > R_{\mathrm{M}}$, because of the fact that photons (bremsstrahlung and annihilation) will travel farther from the shower axis compared to electrons. The published data at similarly low energies are scarce; at 6 GeV, for instance, the comparison between the Monte Carlo and data starts after the depth of $5X_0$, i.e. after the shower maximum [7]. When quoted at shallower depths $(\sim 2X_0)$ by a different study at 1 GeV, the agreement between the data and simulation is poor [8]. In Ref. [9], the simulation underestimates the radial energy escape at 900 MeV—by a factor of two at one R_{M}. This is attributed to the annihilation photons that tend to penetrate larger distances from the shower axis and was not included in the simulations. It is also argued
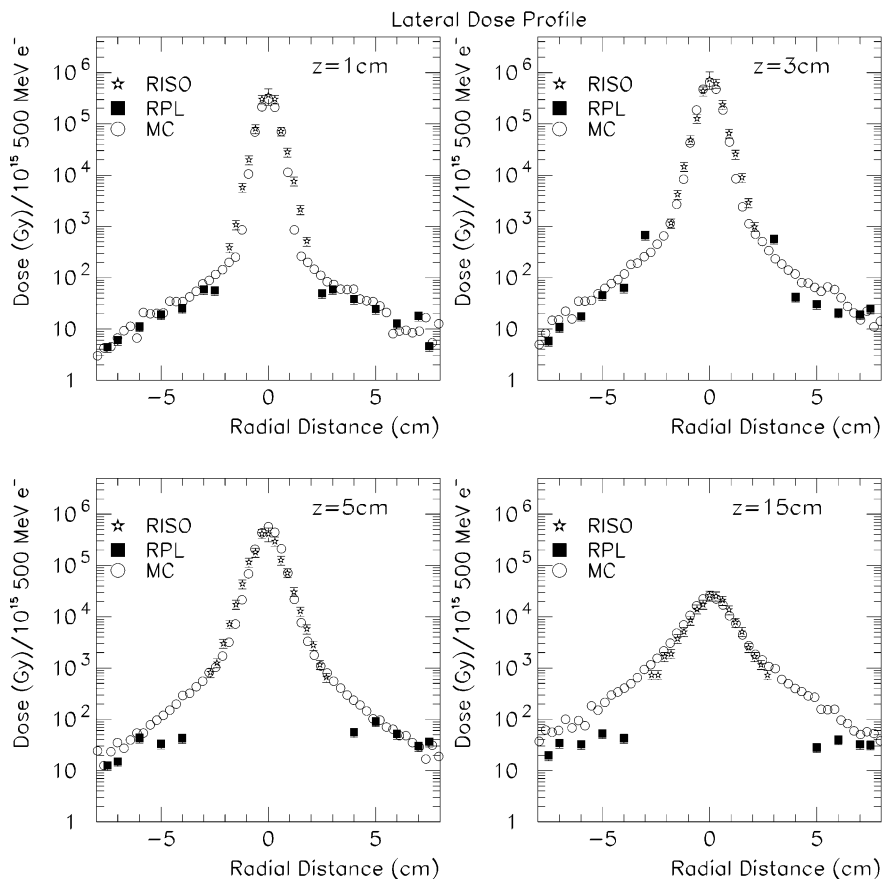

Fig. 4. The longitudinal shower profile is shown at two off-axis shower positions ($r = 0.95$ and 1.95 cm) in iron for 500 MeV electrons. The stars are the RISO paper data and the connected open circles refer to the simulation results.

Fig. 5. The lateral shower profile is shown for four depths ($z = 1, 3, 5$ and 15 cm) in iron for 500 MeV electrons. The black stars and squares are the dosimetry data and the open circles refer to the *EGS4* simulation results.

that the lighter the absorber material, the larger is the disagreement [10].

5. Activation analyses

The reasons for performing activation studies were two-fold: to measure the activation levels of the iron absorber subjected to an intense electron beam and to attempt to measure the longitudinal shower profile using these data. In doing so, we have identified the active isotopes and their levels of activation and also observed that the activation profile along the depth of the detector is a good measure of average gamma profiles and energies

within the absorber. We also attempted to determine the lateral activation profile for a given depth as depicted in Fig. 2

Less than an hour after the irradiation of the Fe I absorber matrix, the activation measurements were carried out to identify the relatively short-lived isotopes using the 0.5-mm thick Fe plates (Fig. 1). The measurements were performed using a 2-in. Ge(Li) detector with 20% relative efficiency. For the long-lived isotopes, the statistical accuracy was better than 3%. Table 4 shows all the identified isotopes for all 12 Fe plates.

Mn^{54} is the most active isotope, contributing $\sim 58\%$ of the total activation near the shower maximum. This isotope is produced by

bremsstrahlung photons via $Fe^{56}(\gamma, np)Mn^{54}$. Fe^{56} is 91.72% naturally abundant. The contribution from the <0.45% trace Mn^{55} in the absorber to Mn^{54} is expected to be about 2.2% when scaled from $Fe^{54}(\gamma, n)Fe^{53}$. Mn^{54} has a 312-day half-life time and emits 835 KeV gammas. Alvarez et al. quote 70 ± 4 mb for maximum cross-section at $E_{max} = 17.4$ MeV [11].

The second highest contributor to the total activation is Fe^{53} via $Fe^{54}(\gamma, n)Fe^{53}$ reaction. Fe^{54}

is 5.8% naturally abundant. The gamma energy threshold for this reaction is 13.8 ± 0.2 MeV [12]. As the photon energy increases, the cross-section sharply increases to a maximum ($\sigma_m \approx 67$ mbarn) and falls again. The strong dependence of the cross-section to gamma energies around $E_m = 18.7$ MeV selects photons in this energy range with full-width half-maximum, $\Gamma = 6.3$ MeV. Norbury et al. studied the same reaction later and quote very similar values [13]. The shape of the curve in Fig. 6 reflects the distribution of photons predominantly in this energy range as a function of absorber depth. When compared with the longitudinal shower shape in Fig. 3, the exponential fall after the shower maximum is in this case slower, indicating that on average, the photons of this energy tend to range over the entire absorber and carry a larger fraction of the shower energy deeper into the absorber compared to electrons. When these β values are compared with the photon mass attenuation lengths, λ_a, there is good agreement. For 2 MeV photons (see Fig. 7),

Table 3
The fit parameters for Mn^{54}, Fe^{53}, Mn^{56} and the total activation curves are listed below. Fig. 6 shows the fits according to Eq. (1)

Isotope	k	α	β (cm^{-1})	z_{max} (cm)
Mn^{54}	2778	2.19	0.34	3.5
Fe^{53}	668	2.35	0.33	4.1
Mn^{56}	211	2.25	0.33	3.8
Total	5651	2.05	0.33	3.2

Table 4
The measured activity of 0.5-mm thick Fe plates placed at different depths in the iron absorber matrix (Fe I). The activity is indicated in KBq where measured. The column numbers correspond to the plate numbers in Fig. 1

| Isotope	1	2	3	4	5	6	7	8	9	10	11	12
Na^{24}		1.4	1.1									
Cl^{38}	1.1	3.3										
Ar^{41}	0.5	2.4	1.7	1.3	1.1	0.5						
K^{42}		18.7	17.1	11.7	8.0							
K^{43}	2.2	6.3	5.4	5.3	2.5							
Sc^{43}	4.6	24.4	23.9	16.0	12.4	8.2	2.7	1.9		0.4		
Sc^{44}	10.3	49.1	47.1	36.3	25.9	13.4	6.4	2.9	1.6	0.7	0.4	
Sc^{44m}	10.1	47.5	45.1	33.1	20.0	11.3	5.8	2.9	1.4	0.6	0.3	0.2
Sc^{46}	15.6	72.5	74.8	59.0	38.6	21.5	11.1	6.7	2.8	1.7	0.9	
Sc^{47}	6.3	29.2	28.3	24.0	17.2	7.8	4.5	2.4	1.2	0.6	0.3	0.2
Cr^{48}	1.4	7.1	7.2	5.8	4.7	2.5	1.1	0.7			0.1	
Sc^{48}	2.2	6.5	5.1	5.1	2.3	1.6	0.8				0.1	
V^{48}	39.1	197.2	203.9	152.1	130.7	69.3	37.0	21.2	10.6	5.5	2.7	1.5
Cr^{49}	12.0	60.2	62.6	55.8	44.7	26.2	15.2	8.2	4.7	2.4	1.3	0.7
Cr^{51}	143.8	768.2	930.6	922.7	772.2	566.3	323.5	202.4	122.7	66.9	37.7	21.3
Fe^{52}	2.3	14.0	18.4	21.1	20.4	16.2	11.3	7.4	4.7	2.7	1.5	1.0
Fe^{53}	45.1	346.1	1148.4	982.1	1069.2	1100.9	562.3	792.0	240.8			45.9
Mn^{52}	31.8	169.5	206.3	197.6	171.1	116.0	66.9	40.4	23.4	12.8	7.1	3.9
Mn^{54}	350.5	2106.7	3084.8	3682.8	3750.1	2970.0	2098.8	1338.5	855.4	502.9	291.9	168.3
Co^{55}	1.3	7.0	7.2	6.2	3.8	1.7		0.9				
Mn^{56}	41.6	166.3	252.7	305.7	322.7	281.2	203.5	136.6	79.6	53.1	32.3	18.7
Total	721.9	4103.4	6171.7	6523.7	6417.6	5237.1	3351.0	2565.3	1348.0	650.2	376.6	262.2
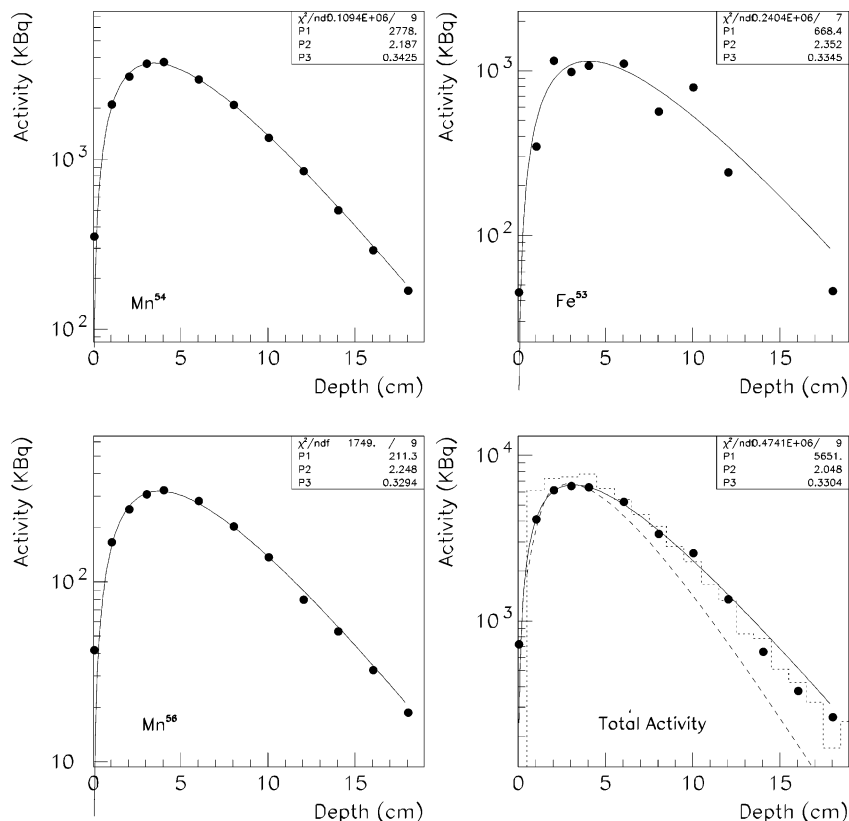
Fig. 6. Mn^{54}, Fe^{53}, Mn^{56} and the total activation profiles as a function of the absorber depth are shown above in KBq and the fit parameters are discussed in the text. The dashed curve in the total activity plot represents the same longitudinal shower profile as in Fig. 3 but is normalized at the shower maximum for contrast. The histogram dotted line, however, is the number of photons ($E_\gamma = 18 \pm 6$ MeV) from *EGS4*, superimposed onto data.

Particle Data Group [5] gives $\lambda_a^{Fe} = 0.33$ cm^{-1} and we measure the same value for βs as shown in Table 3.

The short half-life time (8.51 min) of Fe^{53} made accurate activation measurements difficult and the precision of measurements varied between 2% and 50% for 300 s measurement period. These fluctuations in the measurement can be clearly seen in Fig. 6.

The spectrum of the photons in the shower changes slowly with the depth of the absorber. While the mean photon energy goes from above 10 to 1 MeV in 20 cm iron, the fluctuations around these mean values are large, as *EGS4* results show in Fig. 7. The development of shower is a matter of

balance and fluctuation between the absorbtion of low energy particles and their creation with more energetic secondaries.

The photoproduction of neutrons and protons on complex nuclei strongly depends on energy. At low γ energies ($\sim$ 10–20 MeV), the photons are absorbed via dipole (giant resonance) interactions and (γ, n), (γ, 2n), (γ, np), (γ, p), etc. reactions ensue. These resonance reactions were first predicted by Goldhaber and Teller [14] and by Levinger and Bethe [15]. Cross-sections for about 20 elements were studied experimentally in the early 1950s [12,16,17]. Two generalities emerge in (γ, n) reactions; the maximum cross-section σ_m goes like $A^{5/3}$ where A is the atomic mass and the
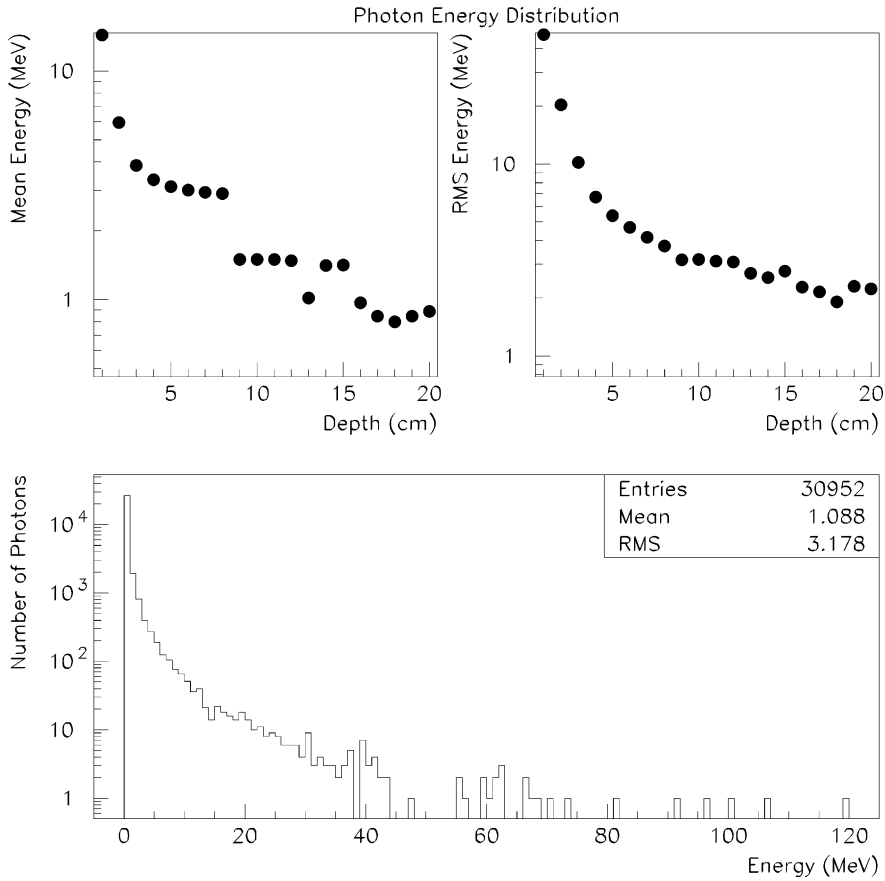
Fig. 7. The *EGS4* simulation for the mean and rms-values of photons in an iron absorber shows a slowly changing energy spectrum as a function of depth for 500 MeV incident electrons. The rms values of the photon energy distributions remain relatively large. In the bottom plot, the photon energies are histogrammed between 10 and 11 cm depth of iron.

measured FWHM, Γ, is about 6 MeV for $A > 30$. At higher energies, the cross-section decreases quickly because only a part of the nucleus interacts with shorter wavelength photons. A common product at these energies is np, photodisintegration of quasi-deuteron, as in the case of $Fe^{56}(\gamma, np)Mn^{54}$. For energies above 50 MeV, the cross-section can be scaled from the known deuteron photodisintegration cross-section, σ_d, in the following form:

$$\sigma(\gamma, np) = L \frac{NZ}{A} \sigma_d \qquad (3)$$

where N and Z are the neutron and proton numbers and A is the atomic mass. Although $6 \leqslant$

$L \leqslant 8$ from theoretical arguments, the experiments suggest $L \approx 3$ [18,19]. The cross-section, σ_d peaks at 4.4 MeV and decreases rapidly, ($\propto 1/E_\gamma$, $E_\gamma \leqslant 125$ MeV), only to rise again at 300 MeV to a less than a 10th of its value at 4.4 MeV. When evaluated at 20 MeV, for example, $\sigma(\gamma, np) \approx 20$ mbarn if $L = 3$ for iron.

The lateral activation profile from Fe II block is shown in Fig. 8. For this particular study only, Fe II block was subjected to 8.5×10^{12} electrons in 20 s and beta activity was measured soon after the termination of irradiation (t_0) and 30 min later in order to identify dominant radioisotopes. Note that at every 2 cm from the shower axis the total activity is down approximately by an order of
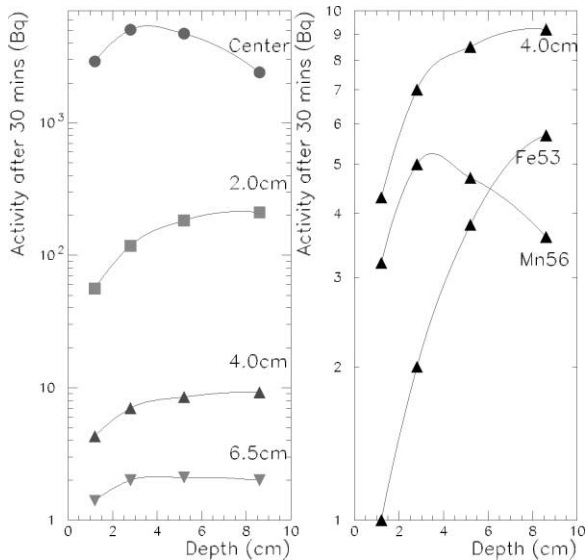
Fig. 8. The total lateral activation profiles for beta emission as a function of off-axis distance are shown on the left plot. The nature of the activity at 4 cm from the shower axis is further shown on the right figure where the uncertainty is estimated to be $\pm 15\%$. See text for details.

highest rapidities. The activation of the iron absorber will reach ~ 60 MBq, if we use a simple conversion of 6 Bq/Gy without being concerned with the short half-life isotopes and activation/deactivation cycles during runs and assume that all of the dose is due to photonuclear reactions. This clearly would be an underestimate.

(2) The *EGS4* simulation reproduces dose measurements fairly well for all depths. The agreement is within 20% at the shower maximum.

(3) A simple parametrization as in Eq. (1) is a reasonable one when an average behavior of the shower is desired, but it is a poor one if precise information is sought at and around the shower maximum.

(4) The lateral shower profile data are well reproduced by the simulation essentially at all depths.

magnitude. When the nature of activity is further analyzed, the major radioisotopes turn out to be Mn^{56} and Fe^{53} with half-lives of 2.58 h and 8.51 min, respectively. The Fe^{53} curve, due to $Fe^{54}(\gamma, n)Fe^{53}$, indicates the distribution of energetic photons as already elaborated above. They tend to penetrate further and spread out from the axis of the cascade. Mn^{56} is mainly due to $Fe^{56} \times (n, p)Mn^{56}$ reaction where the cross-section peaks at $E_n = 14$ MeV–120 mb. The difference between the Fe^{53} and Mn^{56} curves clearly illustrates the energetic photon and neutron distributions in an electromagnetic shower. Activation due to neutrons seems constrained in the upstream end of the absorber and activation due to photonuclear reactions tends deeper and broader in the absorber. We plan to study this phenomena further.

6. Results and discussions

We draw the following conclusions at present:

(1) The CMS forward calorimeter will experience integrated doses up to a Grad or more at the

References

[1] The Hadron Calorimeter Project, Technical Design Report, CERN/LHCC 97-31, 20 June 1997.
[2] N. Akchurin et al., Nucl. Inst. and Meth. A 399 (1997) 202.
[3] CERN Report TIS-CFM/89-14/PP.
[4] J.P. Potier, L. Rinolfi, CERN/PS 98-016 (LP).
[5] C. Caso et al., Particle data group: review of particle physics, Eur. Phys. J. C 3 (1998).
[6] W.R. Nelson, H. Hirayama, D.W.O. Rogers, The EGS4 Code System, SLAC-Report-265.
[7] G. Barthow et al., Nucl. Phys. B 20 (1970) 592.
[8] W.R. Nelson et al., Phys. Rev. 149 (1966) 201.
[9] C.J. Crannel, Phys. Rev. 161 (1967) 310.
[10] T. Yuda et al., Nuovo Cimento 65 (1970) 229; Nucl. Inst. Meth. 73 (1969) 301.

[11] R.A. Alvarez et al., Phys. Rev. C 20 (1979) 128.

[12] L. Katz et al., Phys. Rev. 82 (1951) 271.

[13] J.W. Norbury et al., Aust. J. Phys. 31 (1978) 471.

[14] M. Goldhaber, E. Teller, Phys. Rev 74 (1948) 1046.

[15] J.S. Levinger, H. Bethe, Phys. Rev 78 (1950) 115.

[16] R. Montalbetti et al., Phys. Rev. 91 (1953) 659.

[17] L. Jones, K. Terwilliger, Phys. Rev. 91 (1953) 699.

[18] J.S. Levinger, Nuclear Photo-disintegration, Oxford University Press, Oxford, 1960.

[19] G. Barthow et al., Nucl. Phys. B 2 (1967) 669.